

ChemComm

Chemical Communications

Accepted Manuscript

This article can be cited before page numbers have been issued, to do this please use: D. Jeon, H. Park, J. W. Baek, K. R. Yoon, S. Kim and I. Kim, *Chem. Commun.*, 2026, DOI: 10.1039/D5CC06213F.



This is an Accepted Manuscript, which has been through the Royal Society of Chemistry peer review process and has been accepted for publication.

Accepted Manuscripts are published online shortly after acceptance, before technical editing, formatting and proof reading. Using this free service, authors can make their results available to the community, in citable form, before we publish the edited article. We will replace this Accepted Manuscript with the edited and formatted Advance Article as soon as it is available.

You can find more information about Accepted Manuscripts in the [Information for Authors](#).

Please note that technical editing may introduce minor changes to the text and/or graphics, which may alter content. The journal's standard [Terms & Conditions](#) and the [Ethical guidelines](#) still apply. In no event shall the Royal Society of Chemistry be held responsible for any errors or omissions in this Accepted Manuscript or any consequences arising from the use of any information it contains.

COMMUNICATION

Ultrafast photothermal shock for crystallization of vanadium oxide and in situ anchoring of Co single atoms for enhanced oxygen evolution reaction

Received 00th January 20xx,
Accepted 00th January 20xx

DOI: 10.1039/x0xx00000x

rsc.li/chemcomm

An ultrafast photothermal shock simultaneously crystallizes amorphous vanadium oxide and anchors Co single-atoms, kinetically suppressing atomic aggregation within milliseconds. Featuring a vanadium oxide crystalline phase tunable by the applied shock energy and a photothermal temperature reaching 1600 °C, the resulting self-supported electrode demonstrates a proof-of-concept application as a catalyst for the electrochemical oxygen evolution reaction, establishing an efficient route toward advanced single-atom catalysts.

Single-atom catalysts (SACs) represent a paradigm shift in heterogeneous catalysis, offering the ultimate atom-utilization efficiency and unique electronic properties derived from their low-coordination environment, which can lead to exceptional catalytic activity and selectivity exceeding their nanoparticle counterparts.^{1,2} The performance of SACs is intrinsically linked to the support material, which not only anchors the metal atoms to prevent aggregation but also provides electrochemical robustness and facilitates efficient charge transfer.^{3,4} Beyond structural stabilization, the support often plays an active electronic role by modulating the oxidation state and coordination environment of the anchored atoms through metal–support interactions, defect formation, and charge redistribution at the interface.⁵ Although carbon supports facilitate interfacial charge transfer, their practical application in the oxygen evolution reaction (OER) is severely restricted by their vulnerability to corrosion under high anodic potentials.^{6–8} This limitation has spurred the exploration of more robust transition metal compounds as attractive alternatives capable of optimizing reaction kinetics and ensuring long-term electrochemical stability.^{9–11} Among the vast family, vanadium oxides stand out as an exceptionally promising class of materials for catalytic applications, existing with different stoichiometries

(e.g., V_2O_5 , VO_2 , V_6O_{13} , V_2O_3) due to the multiple accessible oxidation states of vanadium (from +2 to +5).¹² Furthermore, the crystalline phase provides significantly enhanced structural stability and higher intrinsic electronic conductivity compared to its amorphous counterpart, which is essential for ensuring long-term durability and efficient charge transport in an electrocatalytic system.^{13–15} For instance, a recent study has demonstrated that highly crystalline $V_2O_5 \cdot nH_2O$ serve as exceptionally effective hosts for Co SACs, showing significant potential for the OER.¹⁶ This high performance is attributed to the synergistic interaction between the Co sites and the crystalline vanadium oxide support, facilitated by the support's superior structural robustness and well-defined interlayer channels. However, despite this compelling potential, the synthesis of SACs on crystalline vanadium oxide faces a persistent thermodynamic challenge and requires a time-consuming process. The transformation from amorphous vanadium oxide precursors to highly ordered crystalline phases necessitates overcoming substantial activation energy barriers for nucleation and crystal growth, while simultaneously preventing the undesirable, thermodynamically favored aggregation of metal atoms. Conventional equilibrium-driven synthesis routes such as furnace annealing require long-duration thermal treatments (several hours) to achieve high crystallinity.¹⁷ Furthermore, this extended high-temperature exposure promotes undesirable cluster formation, thereby limiting the maximum metal loading achievable in SACs.^{18–20} Consequently, this reliance on time-intensive, equilibrium-based processes highlights a major bottleneck in terms of synthesis efficiency and scalability, leading to a clear need for fundamentally different, non-equilibrium strategies that can simultaneously yield a highly crystalline support and stabilize atomically dispersed catalysts against aggregation.

Our previous work has established ultrafast photothermal shock as a versatile, kinetically controlled non-equilibrium-driven synthesis platform, demonstrating its utility in synthesizing high-entropy alloy on carbon nanofibers (CNFs) as well as anchoring a wide variety of single atoms (e.g., Co, Ni, Pt) onto N-doped graphene supports under ambient conditions,

^a Department of Materials Science and Engineering, Korea Advanced Institute of Science and Technology (KAIST), 291 Daehak-ro, Yuseong-gu, Daejeon 34141, Republic of Korea.

^b Department of Materials Science and Engineering, Konkuk University, 120, Neungdong-ro, Gwangjin-gu, Seoul 05029, Republic of Korea

^c Department of Materials Science and Engineering, Chungnam National University (CNU), 99 Daehak-ro, Yuseong-gu, Daejeon 34134, Republic of Korea.

COMMUNICATION

ChemComm

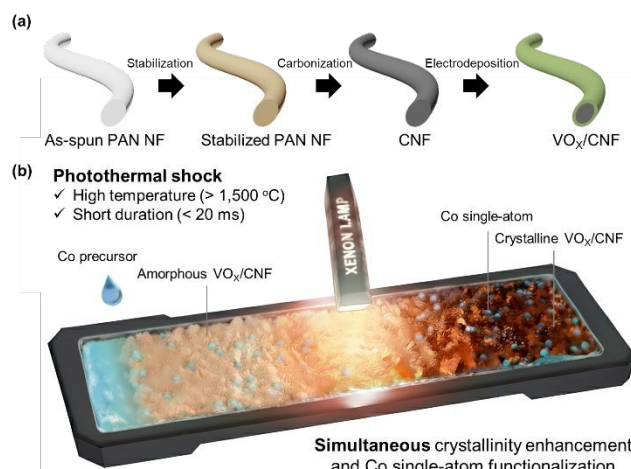


Fig. 1 (a) Schematic illustration of fabrication of amorphous VO_x on CNF. (b) Schematic illustration of the synthesis of Co/ VO_x /CNF via ultrafast photothermal shock process, highlighting the simultaneous crystallinity enhancement and Co single-atom anchoring.

bypassing the need for vacuum systems.^{21,22} More recently, we further extended this strategy to enable the simultaneous, millisecond-scale transformation of nanodiamonds into carbon nanonions and the concurrent anchoring of SACs onto these newly formed nanostructures.²³ Building upon this foundation, herein we apply an ultrafast photothermal shock strategy (1,600 °C within 20 ms), utilizing an intense pulse of light from a Xenon lamp, to fabricate Co SACs anchored on a highly crystalline, electrodeposited vanadium oxide/carbon nanofiber electrode (Co/ VO_x /CNF). The black CNF scaffold absorbs the incident light and converts it into localized heat, thereby photothermally crystallizing the VO_x layer conformally coated on the CNF surface while simultaneously enabling atomically precise anchoring of Co sites. This photothermal shock approach operates on a non-equilibrium timescale, presenting a novel pathway for synthesizing atomically precise active sites on highly crystalline supports, a goal that has been difficult to achieve with conventional time-intensive methods. Finally, we confirm the proof-of-concept application of this material as a durable self-supported electrocatalyst for the OER.

The process begins with the fabrication of the conductive CNF scaffold, where as-spun polyacrylonitrile nanofibers (PAN NFs) are first stabilized at 250 °C for 2 hours and subsequently carbonized at 1,500 °C for 2 hours (Fig. 1). After an O_2 plasma treatment to render the CNF surface hydrophilic (Fig. S1), a uniform, amorphous vanadium oxide layer was conformally coated onto the CNF via a electrodeposition process (Fig. S2a). This method was specifically chosen as it is a simple and robust technique for preparing binder-free electrodes.²⁴ It ensures intimate VO_x –CNF contact, which is crucial for efficient heat transfer during the shock and for optimal electrochemical application. To optimize sufficient loading while preserving electronic conductivity—avoiding the passivation caused by an excessively thick layer (Fig. S2b, S3)—a deposition time of 10 minutes was selected as the optimal condition (VO_x/CNF). Then, VO_x/CNF was confirmed to have a uniform distribution of V and

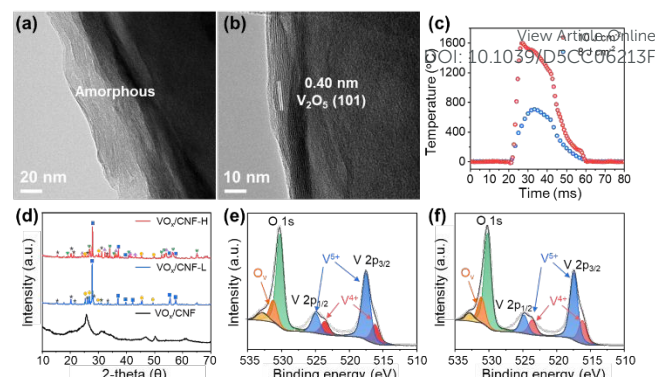


Fig. 2 (a) TEM image of amorphous VO_x /CNF before the shock and (b) crystalline V_2O_5 /CNF after the shock. (c) A temperature-time curve of VO_x /CNF during a 20 ms shock at energy densities of 8 J cm^{-2} (VO_x /CNF-L) and 10 J cm^{-2} (VO_x /CNF-H). (d) XRD pattern of VO_x /CNF, VO_x /CNF-L, and VO_x /CNF-H. (e) XPS spectra of VO_x /CNF-L and (f) VO_x /CNF-H in O 1s and V 2p regions.

O on the CNF support (Fig. S4) with initial vanadium oxidation states of both V^{4+} and V^{5+} (Fig. S5).

The profound structural transformation induced by the photothermal shock was investigated by transmission electron microscopy (TEM). The as-prepared VO_x /CNF, with a 20–40 nm thick VO_x layer electrodeposited on CNF, exhibits the characteristic features of an amorphous structure, lacking any long-range atomic order (Fig. 2a). In contrast, after the application of a single photothermal shock, the VO_x layer undergoes a dramatic transformation into a highly crystalline structure without significant change in its thickness (Fig. 2b). High-resolution TEM imaging clearly reveals well-defined lattice fringes with an interplanar spacing of 0.40 nm, which corresponds to the (101) plane of orthorhombic V_2O_5 . A single 20 ms pulse instantaneously spikes the temperature to approximately 700 °C and 1,600 °C for energy densities of 8 J cm^{-2} and 10 J cm^{-2} (hereafter, denoted as VO_x /CNF-L and VO_x /CNF-H, respectively), providing sufficient activation energy for crystallization followed by rapid cooling (Fig. 2c). Furthermore, the final crystalline phase of the vanadium oxide can be engineered by tuning the applied photothermal energy, as confirmed by the X-ray diffraction (XRD) patterns revealing a clear energy-dependent phase evolution (Fig. 2d). The initial amorphous VO_x /CNF shows only broad halos, indicative of its non-crystalline nature. In contrast, VO_x /CNF-L displays a mixture of crystalline phases, primarily dominated by VO_2 (blue square, JCPDS No. 44-0252), alongside V_2O_5 (gray star, JCPDS No. 41-1426) and V_6O_{13} (yellow circle, JCPDS No. 43-1050). Intriguingly, while VO_x /CNF-H also contains a significant of VO_2 phase, it is further characterized by the emergence of more reduced phases, including V_3O_5 (purple triangle, JCPDS No. 38-1181) and V_2O_3 (green heart, JCPDS No. 34-0187). Moreover, VO_x /CNF-H features slightly lower crystallinity compared to the VO_x /CNF-L, as evidenced by broader XRD peaks (e.g., full width at half maximum (FWHM) of main peak near 27° 2θ is 0.14 vs. 0.12). These combined characteristics are attributed to the effects of the ultrafast heating and cooling process, which

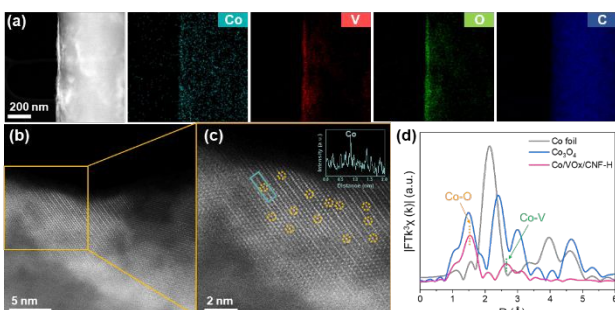


Fig. 3 (a) HAADF-STEM image of Co/VO_x/CNF-H and corresponding elemental distribution maps. (b) High-magnification HAADF-STEM image and (c) magnified image and z-contrast profile of the region highlighted in (b). (d) Fourier transformed k^3 -weighted Co K-edge EXAFS spectra.

inherently generates a high concentration of intrinsic defects.²⁵ Specifically, the high-energy photothermal shock in a carbon-mediated reducing microenvironment strips lattice oxygen to create abundant vacancies that locally disrupt long-range ordering, while the subsequent rapid cooling stabilizes this defect-rich state. This energy-dependent phenomenon is corroborated by X-ray photoelectron spectroscopy (XPS) analysis (Fig. 2e, f). The V 2p spectra reveal an increase in the V⁴⁺/V⁵⁺ area ratio for the VO_x/CNF-H (0.35) compared to VO_x/CNF-L (0.28), while the O 1s concurrently confirm a higher relative area of oxygen vacancies (26.8 % vs. 24.8 %). This simultaneous increase in the relative concentrations of the lower oxidation state (V⁴⁺) and oxygen vacancies provides evidence for the partial reduction of V⁵⁺ induced by the higher shock energy, which aligns with the XRD.

Having confirmed energy-tunable crystallization of the VO_x support, we next investigated simultaneous anchoring of Co SACs during the same ultrafast photothermal shock process. The VO_x/CNF precursor, coated with a Co salt solution, was subjected to the optimized photothermal shock (hereafter, denoted as Co/VO_x/CNF-L (700 °C) and Co/VO_x/CNF-H (1,600 °C), respectively). Notably, the XPS Co 2p binding energy in Co/VO_x/CNF-H exhibits a distinct negative shift compared to Co/VO_x/CNF-L (Fig. S6). This shift provides direct evidence of a strong electronic metal–support interaction (EMSI) mediated by the abundant oxygen vacancies.²⁶ The formation of oxygen vacancies leaves excess delocalized electrons in the lattice, which are transferred to the anchored Co atoms, effectively increasing the electron density on the metal sites. The distribution of the anchored Co atoms of Co/VO_x/CNF-H was confirmed using high-angle annular dark-field scanning transmission electron microscopy (HAADF-STEM) with corresponding energy-dispersive X-ray spectroscopy (EDS) mapping (Fig. 3). The EDS maps show Co signals uniformly distributed with atomic dispersion across the VO_x/CNF surface (Fig. 3a and Fig. S7). HAADF-STEM imaging further verified this, revealing individual Co atoms dispersed on the crystalline vanadium oxide lattice, with no nanoparticles or clusters detected (Fig. 3b, c). To definitively clarify the local environment, Co K-edge Extended X-ray Absorption Fine

Structure (EXAFS) reveals a unique splitting of the first coordination shell into short Co-O1 and long Co-O2 interactions, alongside a distinct Co-V scattering path (Fig. 3d, Fig. S8 and Table S1). This confirms that Co atoms of Co/VO_x/CNF-H are firmly anchored within lattice vacancies, inducing a Jahn-Teller-like distortion and a reduced coordination number characteristic of a defect-trapped state.^{27–29} Importantly, the millisecond-scale thermal cycle is sufficient to generate Co adatoms from the precursor but is insufficient to permit their surface diffusion and aggregation. The subsequent ultrafast cooling rate immobilizes these adatoms at stable anchoring sites, suppressing the thermodynamic drive toward aggregation and stabilizing the Co SACs in its catalytically active, atomically dispersed state. This strategy also proves to be universal, stabilizing not only Co but also Pt, Ru, and Cu SACs on to VO_x/CNF support, in their catalytically active, atomically dispersed states (Fig. S9–S11).

To assess the practical utility as an OER catalyst, we evaluated the electrochemical performance in alkaline medium (1 M KOH). The polarization curves in Fig. 4a illustrate the synergistic effects of the crystalline vanadium oxide support and the Co SACs anchoring. The crystalline phase in VO_x/CNF-L provides slightly enhanced OER activity compared to its amorphous counterpart (amorphous VO_x/CNF), which can be attributed to the improved intrinsic electronic conductivity and structural stability afforded by crystallinity. Notably, anchoring Co SACs on these crystalline supports (Co/VO_x/CNF-H and Co/VO_x/CNF-L) yields a significant boost in OER performance compared to Co-free VO_x/CNF-L, confirming that the atomically dispersed Co moieties act as the primary active sites, while the crystalline nature of the support is crucial for efficient catalysis. Furthermore, Co/VO_x/CNF-H exhibits enhanced OER activity compared to Co/VO_x/CNF-L. The ultrafast cooling from a higher peak temperature (Fig. 2c) limits the time available for attainment of long-range structural order and promotes a higher concentration of oxygen vacancies, which are known to be highly beneficial for OER.^{25,30–31} These oxygen vacancies modulate the local electronic structure of adjacent Co single-atom sites to optimize the adsorption energies of OER intermediates (e.g., *OH, O, OOH) and lower intrinsic kinetic barriers,^{32–34} thereby driving the superior OER performance of Co/VO_x/CNF-H alongside the pronounced reduction phases. Consistent with this, a high Faradaic efficiency of 95.1% was achieved at 100 mA cm⁻² (Fig. S12). Moreover, Co/VO_x/CNF-H shows excellent operational durability (Fig. 4b), maintaining a polarization curve nearly identical to its initial state after 300 cyclic voltammetry (CV) cycles (1.3–1.6 V). Regarding the sustained activity, post-OER XPS Co 2p (Fig. 4c) shows an increased Co³⁺/Co²⁺ ratio, confirming in-situ reconstruction to active CoOOH species.³⁵ This surface activation is accompanied by excellent durability, maintaining a stable potential at 10 mA cm⁻² for over 35 hours (Fig. 4d). This electrochemical robustness is supported by ex situ scanning electron microscopy (SEM) analysis (Fig. S13), showing that the self-supported nanofibrous morphology remained intact after the durability test. Furthermore, HAADF-STEM and EDS analysis verify that the Co species remain atomically



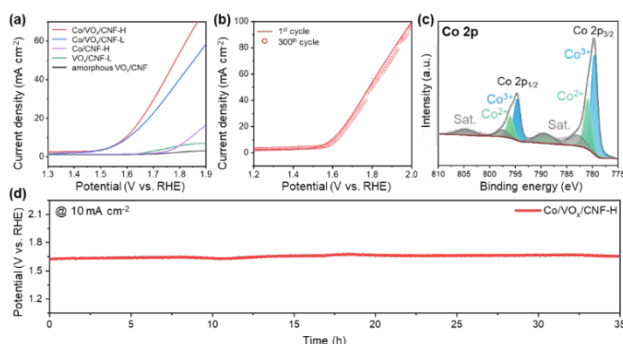


Fig. 4 (a) Polarization curves of Co/VO_x/CNF-H, Co/VO_x/CNF-L, Co/CNF-H, VO_x/CNF-L, and amorphous VO_x/CNF. (b) Polarization curves of Co/VO_x/CNF-H before and after 300 CV cycles. (c) XPS Co 2p spectra of Co/VO_x/CNF-H after 300 CV cycles. (d) Chronopotentiometry curve of Co/VO_x/CNF-H.

dispersed without aggregation, demonstrating the exceptional robustness of the active sites (Fig. S14). Ex situ XPS analysis of the V 2p region after the OER test (Fig. S15) also reveals a significant decrease in the V⁴⁺ peak compared to the as-prepared state (Fig. 2f). This suggests that the less stable, lower-oxidation-state V⁴⁺ species, likely located at the surface, are partially leached or oxidized to V⁵⁺ during the highly oxidative OER. This phenomenon of vanadium leaching from oxide supports under OER conditions is consistent with prior reports.¹⁴ Despite the partial leaching of the vanadium support, the high activity of Co/VO_x/CNF-H is remarkably preserved. This sustained performance provides compelling evidence that the atomically dispersed Co sites, rather than the vanadium oxide support, are the primary active centers for the OER. In this catalytic system, the highly crystalline vanadium oxide framework primarily serves as a robust scaffold to firmly anchor these Co single-atoms through strong Co-O-V interactions. This durability is clear evidence of the strong atomic anchoring achieved via our ultrafast photothermal shock, which robustly anchors the catalytically crucial species against dissolution and aggregation.

In conclusion, we have demonstrated an ultrafast photothermal shock strategy to synthesize Co single atoms anchored on crystalline vanadium oxide. This millisecond process simultaneously achieves the crystallization of the vanadium oxide support and the stable anchoring of Co atoms by kinetically suppressing thermal aggregation. Moreover, the final crystalline phase of the support can be rationally tuned by controlling the energy density. The resulting self-supported electrode successfully served as proof-of-concept application as a durable OER catalyst, presenting a novel and powerful platform for the rational design and scalable fabrication of advanced single-atom catalysts for various energy conversion and storage applications.

This work was supported by the Semiconductor-Secondary Battery Interfacing Platform Technology Development Project of NNFC in 2026 and the National Research Foundation of Korea (NRF) grant funded by the Korea government (MSIT) (No. RS-2024-00435493 and RS-2023-00236572).

Author contributions

View Article Online
DOI: 10.1039/D5CC06213F

D. Jeon: writing, original draft, validation, methodology, and conceptualization. H. Park and J. W. Baek: investigation and editing. K. R. Yoon: editing. S.-J. Kim: editing and supervision. I.-D. Kim: supervision, resources, and funding acquisition.

Conflicts of interest

There are no conflicts to declare.

Data availability

The data supporting this article have been included as part of the Supplementary Information (SI). SI is available. See DOI:

Notes and references

- Y. Pan, X. Wang, W. Zhang, L. Tang, Z. Mu, C. Liu, B. Tian, M. Fei, Y. Sun, H. Su, L. Gao, P. Wang, X. Duan, J. Ma and M. Ding, *Nat. Commun.*, 2022, **13**, 3063.
- H. Jiang, W. Yang, M. Xu, E. Wang, Y. Wei, W. Liu, X. Gu, L. Liu, Q. Chen, P. Zhai, X. Zou, P. M. Ajayan, W. Zhou and Y. Gong, *Nat. Commun.*, 2022, **13**, 6863.
- L. Gloag, S. V. Somerville, J. J. Gooding and R. D. Tilley, *Nat. Rev. Mater.*, 2024, **9**, 173-189.
- Y. Zhang, F. Chen, X. Yang, Y. Guo, X. Zhang, H. Dong, W. Wang, F. Lu, Z. Lu, H. Liu, Y. Xiao and Y. Cheng, *Nat. Commun.*, 2025, **16**, 1956.
- J. Yang, W. Li, D. Wang and Y. Li, *Adv. Mater.*, 2020, **32**, 2003300.
- F.-Y. Chen, Z.-Y. Wu, Z. Adler and H. Wang, *Joule*, 2021, **5**, 1704-1731.
- I. S. Filimonenkov, C. Bouillet, G. Kéranguéven, P. A. Simonov, G. A. Tsirlina and E. R. Savinova, *Electrochimica Acta*, 2019, **321**, 134657.
- J. Bak, H. Kim, S. Lee, M. Kim, E.-J. Kim, J. Roh, J. Shin, C. H. Choi and E. Cho, *ACS Catal.*, 2020, **10**, 12300-12309.
- L. Tang, Y. Wan, Y. Lin, *Chin. J. Struct. Chem.*, 2024, **43**, 100345.
- L. Qin, W. Zhang, R. Cao, *Chin. J. Struct. Chem.*, 2023, **42**, 100105.
- Y. Zhang, B. Wang, C. Hu, M. Humayun, Y. Huang, Y. Cao, M. Negem, Y. Ding, C. Wang, *Chin. J. Struct. Chem.*, 2024, **43**, 100243.
- P. Hu, P. Hu, T. D. Vu, M. Li, S. Wang, Y. Ke, X. Zeng, L. Mai and Y. Long, *Chem. Rev.*, 2023, **123**, 4353-4415.
- M. Hussain, M. Nadeem, H. Sun, S. Karim, A. Nisar, M. Khan and M. Ahmad, *Mater. Chem. Phys.*, 2015, **159**, 19-24.
- S. Prabu, M. Subramani, B. K. Chang and K.-Y. Chiang, *ACS Appl. Nano Mater.*, 2025, **8**, 14083-14094.
- Y.-H. Choi, *Nanomater.*, 2022, **12**, 939.
- C. Youn, S. Shin, K. Shin, C. Kim, C.-L. Park, J. Choi, S. H. Kim, S. Y. Yeo, M. W. Shin, G. Henkelman and K. R. Yoon, *Chem Catal.*, 2022, **2**, 1191-1210.
- M. Kral, V. Prokop, A. A. Kononov, J. R. Pereira, J. Mistrik, A. V. Kolobov, P. J. Fons, Y. Saito, S. Hatayama, Y. Shuang, Y. Sutou, S. A. Rozhkov, Z. R. Stellhorn, S. Hayakawa, I. Pis and F. Bondino, *ACS Appl. Nano Mater.*, 2021, **4**, 8834-8844.
- Y. Wang, C. Li, X. Han, J. Bai, X. Wang, L. Zheng, C. Hong, Z. Li, J. Bai, K. Leng, Y. Lin and Y. Qu, *Nat. Commun.*, 2024, **15**, 5675.
- S. Wang, C. Liu, W. Hao, Y. Zhuang, J. Chen, X. Zhu, L. Wang, X. Niu, J. Mao, D. Ma and Q. Zhao, *Chem. Sci.*, 2025, **16**, 6203-6218.
- C. Rong, K. Flint, C. Doonan and Y. Chen, *Next Mater.*, 2025, **7**, 100457.
- J.-H. Cha, S.-H. Cho, D.-H. Kim, D. Jeon, S. Park, J.-W. Jung, I.-D. Kim and S.-Y. Choi, *Adv. Mater.*, 2023, **35**, 2305222.



22 D.-H. Kim, J.-H. Cha, S. Chong, S.-H. Cho, H. Shin, J. Ahn, D. Jeon, J. Kim, S.-Y. Choi and I.-D. Kim, *ACS Nano*, 2023, **17**, 23347-23358.

23 D. Jeon, H. Shin, J.-H. Cha, H. Kim, S. Park, J. Ahn, S.-H. Cho, C. Park, D.-H. Kim, E. Shin, H. Baik, J. Kim, S.-Y. Choi and I.-D. Kim, *ACS Nano*, 2025, **19**, 34235-34247.

24 R. Velayutham, R. Manikandan, C. J. Raj, A. M. Kale, C. Kaya, K. Palanisamy and B. C. Kim, *J. Alloys Compd.*, 2021, **863**, 158332.

25 Y. Liu, R. Lin, B. Guo, C. Chen, Q. Wu, X. Zhang, Q. Huang, I. S. Amiinu and T. Liu, *Mater. Rep.: Energy*, 2025, 100377.

26 Y. Chen, C. Zhang, D. Yao, O. M. Gazit and Z. Zhong, *ACS Appl. Mater. Interfaces*, 2025, **17**, 3404-3417.

27 A. Gaur, J. Sharma, G. Kaur, S. Mhin, H. Han, *Adv. Funct. Mater.*, 2025, e16674.

28 M. Ji, X. Yang, S. Chang, W. Chen, J. Wang, D. He, Y. Hu, Q. Deng, Y. Sun, B. Li, J. Xi, T. Yamada, J. Zhang, H. Xiao, C. Zhu, J. Li and Y. Li, *Nano Research* 2022, **15**, 1959-1965.

29 D. O. Scanlon, A. Walsh, B. J. Morgan and G. W. Watson, *J. Phys. Chem. C* 2008, **112**, 9903-9911.

30 M. Yonemura, H. Nishibata, R. Fujimura, N. Ooura, K. Hata, K. Fujiwara, K. Kawano, I. Yamaguchi, T. Terai, Y. Inubushi, I. Inoue, T. Yabuuchi, K. Tono and M. Yabashi, *Sci. Rep.*, 2022, **12**, 2237.

31 A. S. Makarov, G. V. Afonin, R. A. Konchakov, J. C. Qiao, A. N. Vasiliev, N. P. Kobelev and V. A. Khonik, *Intermetallics*, 2023, **163**, 108041.

32 Z. Zhang, C. Feng, D. Wang, S. Zhou, R. Wang, S. Hu, H. Li, M. Zuo, Y. Kong and J. Bao, *Nat. Commun.*, 2022, **13**, 2473.

33 M.-Q. Yang, K.-L. Zhou, C. Wang, M.-C. Zhang, C.-H. Wang, X. Ke, G. Chen, H. Wang and R.-Z. Wang, *J. Mater. Chem. A*, 2022, **10**, 25692-25700.

34 C. Rong, K. Dastafkan, Y. Wang and C. Zhao, *Adv. Mater.*, 2023, **35**, 2211884.

35 Z. Xiao, Y.-C. Huang, C.-L. Dong, C. Xie, Z. Liu, S. Du, W. Chen, D. Yan, L. Tao, Z. Shu, G. Zhang, H. Duan, Y. Wang, Y. Zou, R. Chen and S. Wang, *J. Am. Chem. Soc.* 2020, **142**, 12087-12095

View Article Online
DOI: 10.1039/D5CC06213F



Data availability statement

The data supporting this article have been included as part of the Supplementary Information (SI). SI is available.

See DOI: